



Silica-coated magnetic nanoparticles induce glucose metabolic dysfunction in vitro via the generation of reactive oxygen species

Tae Hwan Shin¹ · Chan Seo² · Da Yeon Lee¹ · Moongi Ji² · Balachandran Manavalan¹ · Shaherin Basith¹ · Suresh Kumar Chakkarapani³ · Seong Ho Kang^{3,4} · Gwang Lee¹ · Man Jeong Paik² · Chan Bae Park¹

Received: 23 October 2018 / Accepted: 31 January 2019 / Published online: 8 February 2019
© The Author(s) 2019

Abstract

Nanoparticles are a useful material in biomedicine given their unique properties and biocompatibility; however, there is increasing concern regarding the potential toxicity of nanoparticles with respect to cell metabolism. Some evidence suggests that nanoparticles can disrupt glucose and energy homeostasis. In this study, we investigated the metabolomic, transcriptomic, and integrated effects of silica-coated magnetic nanoparticles containing rhodamine B isothiocyanate dye [MNPs@SiO₂(RITC)] on glucose metabolism in human embryonic kidney 293 (HEK293) cells. Using gas chromatography–tandem mass spectrometry, we analysed the metabolite profiles of 14 organic acids (OAs), 20 amino acids (AAs), and 13 fatty acids (FAs) after treatment with 0.1 or 1.0 µg/µl MNPs@SiO₂(RITC) for 12 h. The metabolic changes were highly related to reactive oxygen species (ROS) generation and glucose metabolism. Additionally, effects on the combined metabolome and transcriptome or “metabotranscriptomic network” indicated a relationship between ROS generation and glucose metabolic dysfunction. In the experimental validation, MNPs@SiO₂(RITC) treatment significantly decreased the amount of glucose in cells and was associated with a reduction in glucose uptake efficiency. Decreased glucose uptake efficiency was also related to ROS generation and impaired glucose metabolism in the metabotranscriptomic network. Our results suggest that exposure to high concentrations of MNPs@SiO₂(RITC) produces maladaptive alterations in glucose metabolism and specifically glucose uptake as well as related metabolomic and transcriptomic disturbances via increased ROS generation. These findings further indicate that an integrated metabotranscriptomics approach provides useful and sensitive toxicological assessment for nanoparticles.

Keywords Gas chromatography–tandem mass spectrometry · Glucose uptake · Magnetic nanoparticles · Nanotoxicity · Reactive oxygen species

Tae Hwan Shin and Chan Seo contributed equally to this work.

Electronic supplementary material The online version of this article (<https://doi.org/10.1007/s00204-019-02402-z>) contains supplementary material, which is available to authorized users.

✉ Man Jeong Paik
paik815@scnu.ac.kr

✉ Chan Bae Park
chanbaepark@ajou.ac.kr

¹ Department of Physiology, Department of Biomedical Sciences, Ajou University School of Medicine, 164, World cup-ro, Yeongtong-gu, 16499 Suwon, Republic of Korea

Introduction

Nanoparticles (NPs) are increasingly used for diagnostic and treatment purposes in biomedicine (Jain and Stylianopoulos 2010; Qi et al. 2017; Stark 2011). Magnetic nanoparticles (MNPs) and MNPs coated with biocompatible compounds such as silica, polyethylene glycol, and polysaccharides are used in vivo as tracers, contrast agents for magnetic resonance

² College of Pharmacy, Suncheon National University, Suncheon, Republic of Korea

³ Department of Chemistry, Graduate School, Kyung Hee University, Yongin-si, Republic of Korea

⁴ Department of Applied Chemistry and Institute of Natural Sciences, Kyung Hee University, Yongin-si, Republic of Korea

imaging (MRI)-based cell labelling, and transfection agents (Delyagina et al. 2014; Ding et al. 2018; Ito et al. 2006; Silva et al. 2017; Yoon et al. 2005). However, the nature and underlying cellular mechanisms of NP toxicity remain unclear.

Previous studies have demonstrated that internalised NPs induce cytotoxicity by stimulating ROS production and oxidative protein modification, alterations in redox-regulation, and mitochondrial dysfunction (Krug and Wick 2011; Meng et al. 2009; Phukan et al. 2016). Under physiological conditions, these disturbances are associated with functional alterations in cellular metabolism. Indeed, glucose and energy metabolic dysfunction after NP exposure can potentially contribute to disease occurrence (Lai et al. 2015) and renal cytotoxicity (Iavicoli et al. 2016). The kidneys play an important role in glucose homeostasis by filtering and reabsorbing ~ 180 g of glucose per day in humans (DeFronzo et al. 2012). Impaired glucose uptake in the kidneys leads to glycosuria, a general state of imbalanced glucose homeostasis with symptoms similar to those of diabetes mellitus and Fanconi–Bickel syndrome (Bahillo-Curieses et al. 2017; Cersosimo et al. 2014). However, the effects of NPs on glucose metabolism are poorly understood on a cellular level.

We previously demonstrated that exposure to MNPs@SiO₂(RITC) altered the expression of cellular metabolism-related genes and produced metabolic disturbances in organic acids (OAs) and amino acids (AAs) in HEK293 cells using gas chromatography mass spectrometry (Shim et al. 2012; Yoon et al. 2005). Importantly, the metabolic profiling of OAs, AAs, and fatty acids (FAs) as an end-point biological phenotype (Gibney et al. 2005) can reflect important changes in cellular processes. However, there are few methods available for the amplification of very low-abundance metabolites, and quantitative analyses of targeted methods provide only a partial representation of metabolism in the cell (Van Assche et al. 2015). New approaches integrating transcriptomics and metabolomics provide a more powerful and comprehensive analysis of treatment outcomes after NP exposure compared to classical methods for the analysis of nanotoxicity (Shin et al. 2018).

In this study, we performed a comprehensive evaluation of MNPs@SiO₂(RITC)-induced toxicity in vitro. We analysed changes in OAs, AAs, and FAs using gas chromatography–tandem mass spectrometry (GC-MS/MS) and disturbances in the transcriptome using a microarray in MNPs@SiO₂(RITC)-treated cells. Finally, we applied a metabotranscriptomics approach to better inform the nature and mechanisms of MNPs@SiO₂(RITC) nanotoxicity.

Materials and methods

Chemicals and reagents

Standards for 14 OAs (3-hydroxybutyric acid, pyruvic acid, acetoacetic acid, lactic acid, glycolic acid, 2-hydroxybutyric acid, malonic acid, succinic acid, fumaric acid, oxalacetic acid, 2-ketoglutaric acid, malic acid, 2-hydroxyglutaric acid, and citric acid), 20 AAs (alanine, glycine, valine, leucine, isoleucine, proline, γ -aminobutyric acid, pyroglutamic acid, methionine, serine, phenylalanine, cysteine, aspartic acid, glutamic acid, asparagine, ornithine, glutamine, lysine, tyrosine, and tryptophan), and 13 FAs (myristoleic acid, myristic acid, palmitoleic acid, palmitic acid, linoleic acid, oleic acid, stearic acid, arachidonic acid, arachidic acid, behenic acid, nervonic acid, lignoceric acid, and cerotic acid); ethyl chloroformate (ECF); methoxyamine hydrochloride; and trimethylamine (TEA) were purchased from Sigma-Aldrich (St. Louis, MO, USA). *N*-methyl-*N*-(*tert*-butyldimethylsilyl) trifluoroacetamide (MTBSTFA) was obtained from Pierce (Rockford, IL, USA). Toluene, diethyl ether, ethyl acetate, dichloromethane, and sodium chloride were supplied by Kanto Chemical (Tokyo, Japan).

MNPs@SiO₂(RITC)

MNPs@SiO₂(RITC) consisted of a ~9-nm cobalt ferrite core (CoFe₂O₃) that was chemically bonded to rhodamine isothiocyanate dye (RITC) and coated with a silica shell (Phukan et al. 2016; Shim et al. 2012; Yoon et al. 2005) and was provided from BITERIALS (Seoul, South Korea). The size of the NP was 50 nm in diameter and MNPs@SiO₂(RITC) was previously reported to have a zeta potential between –40 and –30 mV (Beck et al. 2012; Yoon et al. 2005). A previous study determined that the MCF-7 cell line internalised ~ 10⁵ particles of MNPs@SiO₂(RITC) per cell using inductively coupled plasma atomic emission spectrometry (Yoon et al. 2005). The dosage used in this study was determined by treating HEK293 cells with MNPs@SiO₂(RITC) at concentrations ranging from 0.01 to 2.0 $\mu\text{g}/\mu\text{l}$ for 12 h and calculating the uptake efficiency at each concentration (Shim et al. 2012). The optimal concentration of MNPs@SiO₂(RITC) for in vitro use was 0.1 $\mu\text{g}/\mu\text{l}$, consistent with its safe use for MRI contrast in human cord blood-derived mesenchymal stem cells (Park et al. 2010). Disturbances of gene expression and metabolic profiles at this concentration were similar to those in control HEK293 cells (Shim et al. 2012). The uptake efficiency of MNPs@SiO₂(RITC) plateaued at 1.0 $\mu\text{g}/\mu\text{l}$. Therefore, we used 0.1 $\mu\text{g}/\mu\text{l}$ to represent a normal or low

dose and 1.0 $\mu\text{g}/\mu\text{l}$ to represent an overdose of NPs in the present study. Additionally, we verified that the off-target biological effects of MNPs@SiO₂(RITC) after treatment of HEK293 cells for 48 h were induced by the shell rather than the cobalt ferrite core (Phukan et al. 2016; Shin et al. 2018).

Cell culture

Human embryo kidney 293 (HEK293) cells were used to analyze the nanotoxicity of MNPs@SiO₂(RITC) as HEK293 has been well studied for its relation to silica nanoparticle-induced cytotoxicity and the renal toxicity models (Wang et al. 2009; Zhang et al. 2015). HEK293 cells were obtained from the American Type Culture Collection. Cells were cultured in Dulbecco's high-glucose modified Eagle's medium (DMEM, Gibco, USA) supplemented with 10% foetal bovine serum (Gibco), 100 units/ml penicillin, and 100 $\mu\text{g}/\text{ml}$ streptomycin (Gibco) and incubated in a humidified atmosphere of 5% CO₂ at 37 °C.

Preparation of standard solutions

Standard stock solutions (10 $\mu\text{g}/\mu\text{l}$) were individually prepared for OAs including 3,4-dimethoxybenzoic acid as an internal standard, AAs including norvaline as an internal standard in 0.1 M HCl, and FAs including pentadecanoic acid as internal standard in methanol. Working solutions of 0.01 and 0.1 $\mu\text{g}/\mu\text{l}$ were then prepared by diluting each AA stock solution with 0.1 M HCl and each OA and FA stock solution with methanol. All standard solutions were stored at 4 °C until use.

GC-MS/MS

The GC-MS/MS analysis was performed with a Shimadzu 2010 Plus gas chromatograph interfaced with a Shimadzu TQ 8040 triple quadrupole mass spectrometer (Shimadzu, Kyoto, Japan) equipped with an Ultra-2 (5% phenyl-95% methylpolysiloxane bonded phase; 25 m \times 0.20 mm ID, 0.11 μm film thickness) cross-linked capillary column (Agilent Technologies, Atlanta, GA, USA). Samples were introduced in split-injection mode (10:1). The oven temperature was initially set to 60 °C for 2 min, increased to 255 °C at a rate of 25 °C/min, and further increased to 300 °C at a rate of 7 °C/min with a holding time of 2.5 min. The temperatures of the injector, interface and ion source were 260 °C, 300 °C, and 230 °C, respectively. Helium (0.5 ml/min, constant flow mode) and argon were used as carrier and collision gases, respectively. Ionization used the electron ionization (EI) mode set to 70 eV.

Sample preparation for OA, AA, and FA profiling in vitro

We performed profiling analyses of 14 OAs, 20 AAs, and 13 FAs as EOC/MO/TBDMS derivatives on GC-MS/MS (Paik and Kim 2004; Paik et al. 2005). Briefly, cells were homogenised by freeze-thawing and 1.0 ml of distilled water containing 0.1 μg of 3,4-dimethoxybenzoic acid, norvaline, and pentadecanoic acid was added to each sample. Each aliquot solution was adjusted to a pH \geq 12 with 5.0 M sodium hydroxide in dichloromethane (2.0 ml) containing ECF (40 μl), which was converted to the EOC derivative and subsequently the MO derivative by reaction with methoxyamine hydrochloride at 60 °C for 60 min. The aqueous phase was acidified (pH \leq 2.0 with 10% sulphuric acid), saturated with sodium chloride, and extracted twice with diethyl ether and ethyl acetate (3 ml \times 2). The extracts were evaporated to dryness using a gentle nitrogen stream. Dry residues containing OAs, AAs, and FAs were reacted with TEA (5 μl), toluene (20 μl), and MTBSTFA (20 μl) at 60 °C for 30 min to form TBDMS derivatives.

Metabotranscriptomic data analysis

Differences in gene expression were examined using the Affymetrix system (ISTECH, South Korea) in conjunction with the Human U133 Plus 2.0 50K microarray, which contains 54,675 probes. Between-group differences in the data distributions were analysed with GenPlex 3.0 software as previously described (Shim et al. 2012) and probe signals were quantile normalised. Profiles of OAs, AAs, and FAs were imported from GC-MS/MS data. Biological pathways and functions were identified using web-based bioinformatics software (IPA; Ingenuity Systems, USA). We used \pm 3.0-fold change for genes and \pm 1.2-fold change for metabolites as cut-offs to generate data sets of genes and metabolites that were significantly different between the untreated control and MNPs@SiO₂(RITC)-treated groups.

Determination of glucose uptake efficiency and concentration in cells and media

Uptake efficiency and amounts of glucose were quantified using a luciferase-based kit in accordance with manufacturer specifications (Promega, USA). Briefly, cells were treated with 0.1 or 1.0 $\mu\text{g}/\mu\text{l}$ MNPs@SiO₂(RITC) for 12 h in a 384-well white plate (Corning, CA). After incubation, cells were washed twice with phosphate buffered saline (PBS). For the determination of glucose uptake, cells were incubated with 1 mM 2-deoxyglucose (2DG) for 10 min. The uptake of 2DG was stopped with an acid detergent solution (Stop buffer, described in the manufacturer's protocol) and cells were subjected to lysis. The pH was neutralised with a high-pH buffer

solution (Neutralization buffer, described in the manufacturer's protocol) for enzymatic reaction. Then, lysates were mixed with G6PDH, nicotinamide adenine dinucleotide phosphate (NADP⁺), reductase for proluciferin, ATP, and luciferase. G6PDH oxidized 2DG6P to 6-phosphodeoxygluconate and simultaneously reduced NADP⁺ to NADPH, and the reductase converted proluciferin to luciferin using NADPH. Thus, the assay end-point was luciferase luminescence. The end-point luminescence was recorded using a 0.3–1 s integration on a Synergy 2 luminometer (BioTek, CA) and subsequently captured using a ChemiDoc™ Touch Gel Imaging System (Bio-Rad).

To visualize the efficiency of glucose uptake into cells, they were treated with 0.1 or 1.0 µg/µl MNPs@SiO₂(RITC) for 12 h in cover slips. After treatment, cells were treated with fluorescent d-glucose analogue 2-[N-(7-nitrobenz-2-oxa-1,3-diazol-4-yl)amino]-2-deoxy-d-glucose (2-NBDG) at 37 °C for 30 min and the fluorescence associated with 2-deoxy-d-glucose was observed by fluorescence microscopy (Axiovert 200M, Carl Zeiss, Jena, Germany).

To determine the amount of glucose in cells, cells were treated with 0.1 or 1.0 µg/µl MNPs@SiO₂(RITC) and subsequently washed twice with PBS. Cellular activities were stopped with a stop buffer and neutralised with neutralization buffer. The lysates were mixed with glucose dehydrogenase, NADP⁺, reductase for proluciferin, ATP, and luciferase. Glucose in the media was measured after 400-fold dilution with PBS. Glucose dehydrogenase oxidized glucose to glucono-1,5-lactone and simultaneously reduced NADP⁺ to NADPH, and the reductase converted proluciferin to luciferin using NADPH. The produced luciferin was oxidized by luciferase, generating luminescent. End-point luminescence was recorded using a 0.3–1-s integration on a Synergy 2 luminometer (BioTek, CA) and subsequently captured using a ChemiDoc™ Touch Gel Imaging System (Bio-Rad).

RNA isolation and quantitative real-time PCR

Total RNA was isolated from cells using RNazol B (Tel-Test, USA). Briefly, cells treated with 0.1 or 1.0 µg/µl MNPs@SiO₂(RITC) for 12 h and untreated control cells (2×10^6 cells) were harvested in RNazol B solution followed by the addition of chloroform and incubation for 5 min on ice. Cells were then treated with isopropyl alcohol to precipitate total RNA. Pellets were washed in 70% ethanol followed by air drying, and total RNA was dissolved with RNase-free water. RNA purity was determined with optical density values of 1.8–2.0 at wavelength ratios of 260/230 and 260/280 using spectrophotometry (Eppendorf, Hamburg, Germany). A cDNA library was synthesised using the iScript Advanced cDNA Synthesis Kit (Bio-Rad). The reaction conditions were as follows: 46 °C for 20 min followed by 95 °C for 1 min.

The expression levels of metabotranscriptomic network-related genes were detected by qPCR using the SsoAdvanced™ Universal SYBR® Green Supermix real-time PCR kit (Bio-Rad) with gene-specific primer pairs (Supplementary Table 1) on a Rotor Gene-Q system (Qiagen, CA). The reaction conditions were as follows: 95 °C for 5 min followed by 50 cycles of 95 °C for 5 s and 60 °C for 30 s. The threshold/quantification cycle (Ct/Cq) value was determined at the point where the detected fluorescence was statistically higher than the background level. PCR products were analysed based on a melting curve constructed using Rotor-Gene 1.7 software (Qiagen). PCR was prepared as independent triplicate samples. The relative quantification of target gene expression was performed using the $2^{-\Delta\Delta C_t}$ method.

Statistical analysis

The results were analysed with a one-way analysis of variance (ANOVA) and Tukey's honestly significant difference (HSD) post hoc tests using IBM-SPSS software (IBM Corp., USA). Differences were considered to be statistically significant when $p < 0.05$. The composition levels of AA, OA, and FA in each group were compared using a supervised multivariate PCA using R statistical software (<https://www.R-project.org>).

Results

Metabolic disturbance in MNPs@SiO₂(RITC) treated cells analysed by GC-MS/MS

Metabolic changes in AAs, OAs, and polyamines in MNPs@SiO₂(RITC)-treated cells are significantly associated with the generation of ROS (Phukan et al. 2016; Shim et al. 2012). In this study, we performed profiling analyses of 14 OAs, 20 AAs, and 13 FAs using EOC/MO/TBDMS derivatisation and GC-MS/MS analyses of cells treated with 0.1 or 1.0 µg/µl MNPs@SiO₂(RITC) (Supplementary Table 2). Eleven of 14 OAs were positively detected at baseline. Seven OAs, 8 AAs, and 6 FAs were significantly affected by treatment with 1.0 µg/µl MNPs@SiO₂(RITC), and 5 OAs, 6 AAs, and 4 FAs were significantly affected by treatment with 0.1 µg/µl MNPs@SiO₂(RITC) compared to an untreated control condition.

Metabolite ratio values were calculated as the change in metabolite level in MNPs@SiO₂(RITC)-treated cells divided to the mean corresponding control value. Moreover, we performed a principal component analysis (PCA) of all 44 metabolites in the untreated control, 0.1, and 1.0 µg/µl MNPs@SiO₂(RITC) conditions and used 3 principal components, i.e., PC1, PC2, and PC3, to construct

three-dimensional score plots (Supplementary Fig. 1). Three distinct clusters and 3 PCs accounted for 83.2% of the total variance in the raw data. Untreated control cell clusters were visibly different from those of MNPs@SiO₂(RITC)-treated cells, and this difference was most evident in a comparison of the untreated control and 1.0 µg/µl MNPs@SiO₂(RITC)-treated cell clusters.

A visual star symbol plot was drawn using the metabolite ratio values and rays of the plot based on Supplementary Table 2 (Fig. 1). Star shapes representing the MNPs@SiO₂(RITC) treatment groups were readily distinguishable from that of the untreated control group mean. With regard to OA profiles, 1.0 µg/µl MNPs@SiO₂(RITC) treatment was associated with decreased levels of 3-hydroxybutyric, acetoacetic, succinic, oxaloacetic, 2-hydroxyglutaric, and citric acids and increased levels of pyruvic acid (Fig. 1a). Similarly, 0.1 µg/µl MNPs@SiO₂(RITC) treatment was associated with decreased levels of pyruvic, acetoacetic, oxaloacetic, and citric acids and increased level of malic acid. Common differences were more pronounced in the 1.0 µg/µl MNPs@SiO₂(RITC) treatment group.

With regard to AA profiles, 1.0 µg/µl MNPs@SiO₂(RITC) treatment was associated with decreased levels of glycine, serine, cysteine, and glutamine and increased levels of leucine, glutamic acid, lysine, and tyrosine (Fig. 1b). Similarly, 0.1 µg/µl MNPs@SiO₂(RITC) treatment was associated with decreased levels of glutamine and tryptophan and increased levels of leucine, serine, glutamic acid, and lysine. Common differences were more pronounced in the 1.0 µg/µl MNPs@SiO₂(RITC) treatment group.

With regard to FA profiles, 1.0 µg/µl MNPs@SiO₂(RITC) treatment was associated with decreased levels of myristoleic, palmitoleic, and linoleic acids and increased levels of arachidonic, behenic, and lignoceric acids (Fig. 1c). Similarly, 0.1 µg/µl MNPs@SiO₂(RITC) treatment was associated with decreased levels of myristoleic, palmitoleic, and linoleic acids and increased levels of arachidonic acid.

Changes were similar between the 0.1 and 1.0 µg/µl MNPs@SiO₂(RITC) groups and more pronounced in the 1.0 µg/µl MNPs@SiO₂(RITC) group, except for palmitoleic acid.

Metabolomic network associated with ROS generation and glucose metabolic dysfunction after MNPs@SiO₂(RITC) treatment

Based on the metabolic profiles, we generated a metabolomics network using a bioinformatics tool, the ingenuity pathway analysis (IPA). Considering the physiological state and most significant changes in metabolic profiles after MNPs@SiO₂(RITC) treatment, we postulated that a ± 1.2 -fold change would be an adequate cut-off to reflect abnormal conditions. There was a clear network of metabolic relationships among OAs, AAs, and FAs in the 1.0 µg/µl MNPs@SiO₂(RITC)-treated group compared to the 0.1 µg/µl MNPs@SiO₂(RITC)-treated and untreated control groups (Fig. 2 and Supplementary Fig. 2). Biological changes including ROS generation and glucose metabolic dysfunction were deduced from the metabolic profile. Increased ROS generation and glucose metabolic dysfunction were predicted after treatment with 1.0 µg/µl MNPs@SiO₂(RITC) (Supplementary Fig. 3).

Representative selected-ion monitoring (SIM) chromatograms of 3 influential OAs (pyruvic acid, acetoacetic acid, and succinic acid), 4 influential AAs (glycine, cysteine, aspartic acid, and glutamic acid), and 2 influential FAs (linoleic acid and arachidonic acid) in the metabolomic network are shown in Fig. 3.

Generation of the metabotranscriptomic network and evaluation of glucose homeostasis in MNPs@SiO₂(RITC)-treated cells

The proposed metabolic network and subsequent predictions were only based on an end-point phenotype with limited

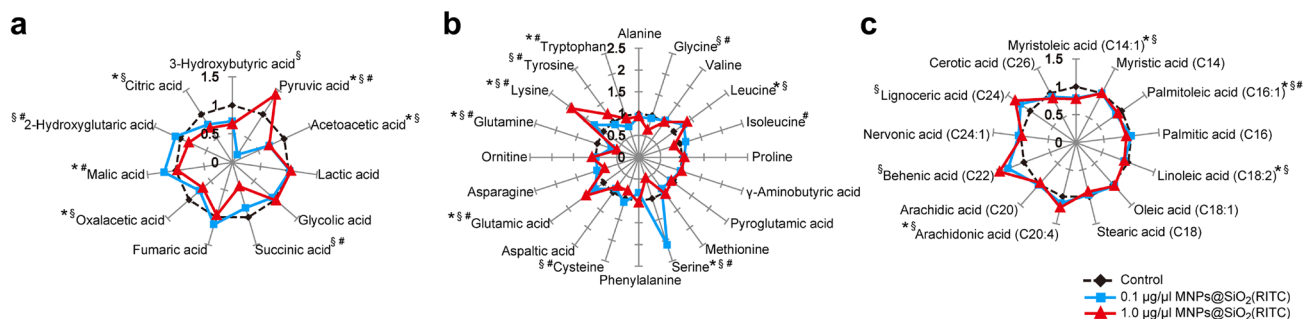


Fig. 1 Metabolic disturbance in MNPs@SiO₂(RITC)-treated HEK293 cells. Star patterns for 11 organic acids (OAs; **a**), 20 amino acids (AAs; **b**), and 13 fatty acids (FAs; **c**) in HEK293 cells treated with 0.1 or 1.0 µg/µl MNPs@SiO₂(RITC) and untreated control

cells. * $p < 0.05$ untreated control vs. 0.1 µg/µl MNPs@SiO₂(RITC), § $p < 0.05$ untreated control vs. 1.0 µg/µl MNPs@SiO₂(RITC), and # $p < 0.05$ 0.1 µg/µl vs. 1.0 µg/µl MNPs@SiO₂(RITC)

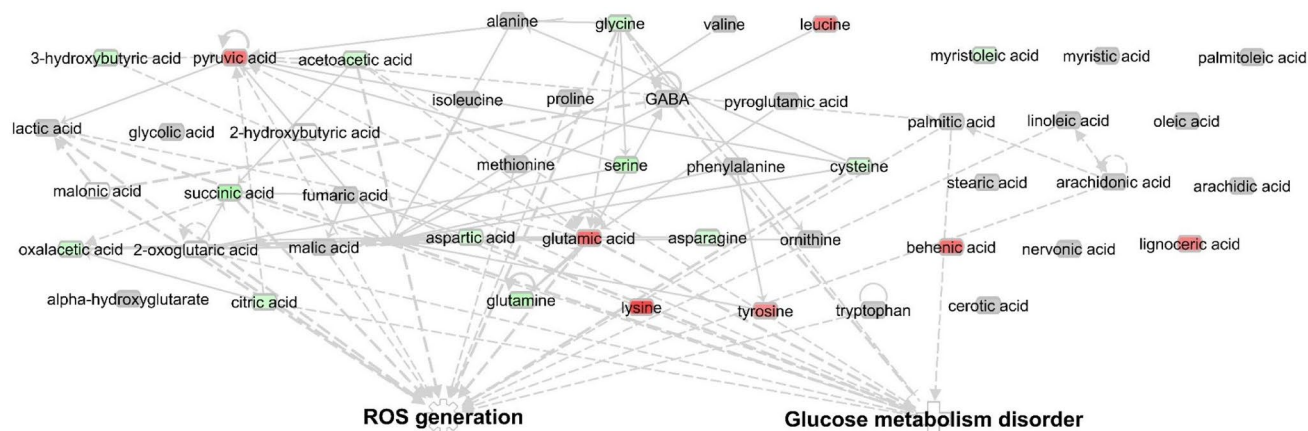


Fig. 2 Metabolomic network of 1.0 $\mu\text{g}/\mu\text{l}$ MNPs@SiO₂(RITC)-treated HEK293 cells. The analysis employed a fold-change cut-off value of ± 1.2 . Red and green areas indicate metabolite concentra-

tions that were increased and decreased compared to the untreated control group, respectively. (Colour figure online)

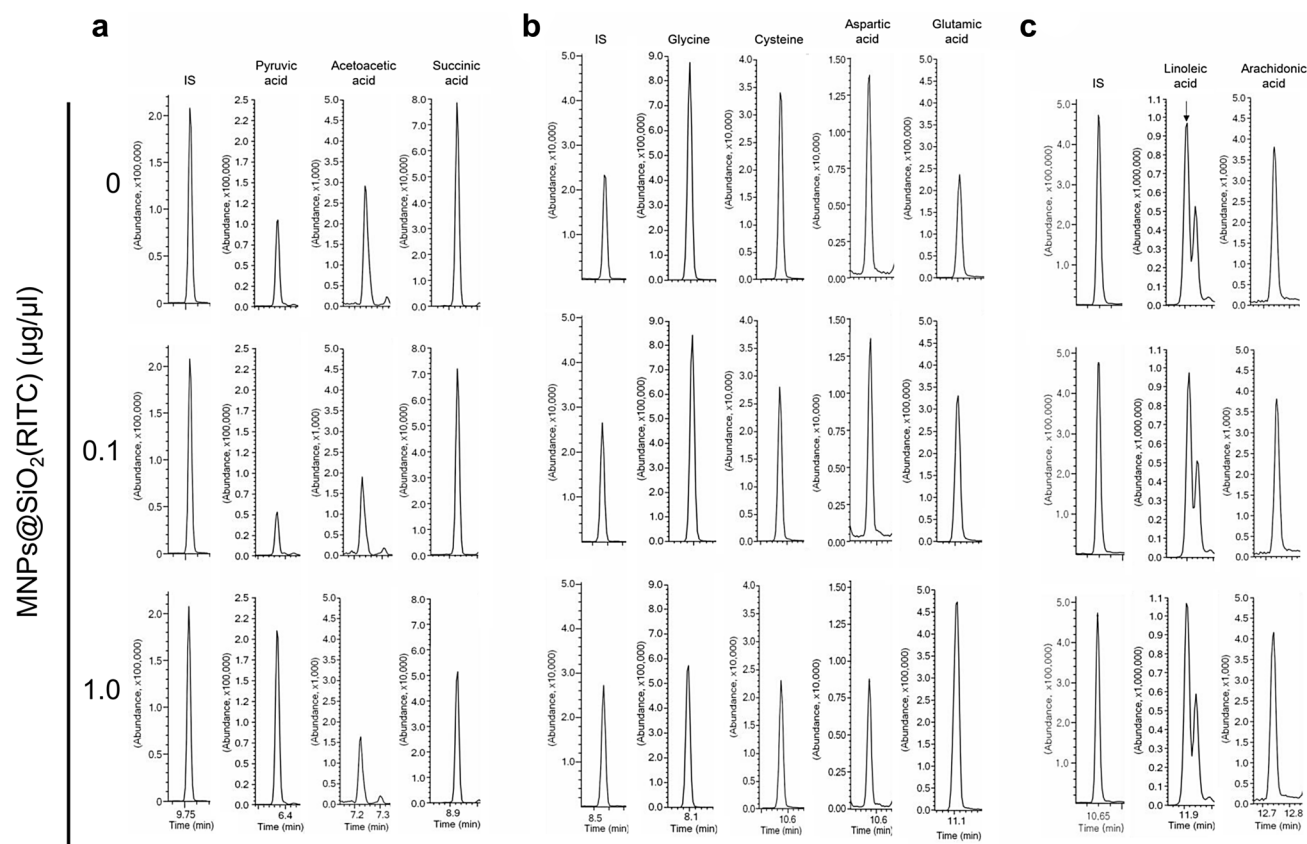


Fig. 3 Representative selected-ion monitoring chromatograms of influential metabolites. **a** Three organic acids (OAs; pyruvic acid, acetoacetic acid, and succinic acid), **b** 4 amino acids (AAs; glycine, cysteine, aspartic acid, and glutamic acid), and **c** 2 fatty acids

(linoleic acid and arachidonic acid) in the metabolomic network. IS, internal standard (3,4-dimethoxybenzoic acid for OAs, norvaline for AAs, and pentadecanoic acid for FAs)

capacity to reflect actual biological processes (Evans 2015; Rehrauer et al. 2013). To compensate for potential weakness in the proposed metabolomic network, we generated

a transcriptomic network associated with ROS generation and glucose metabolic dysfunction and integrated this information to yield a metabotranscriptomic network (Fig. 4a,

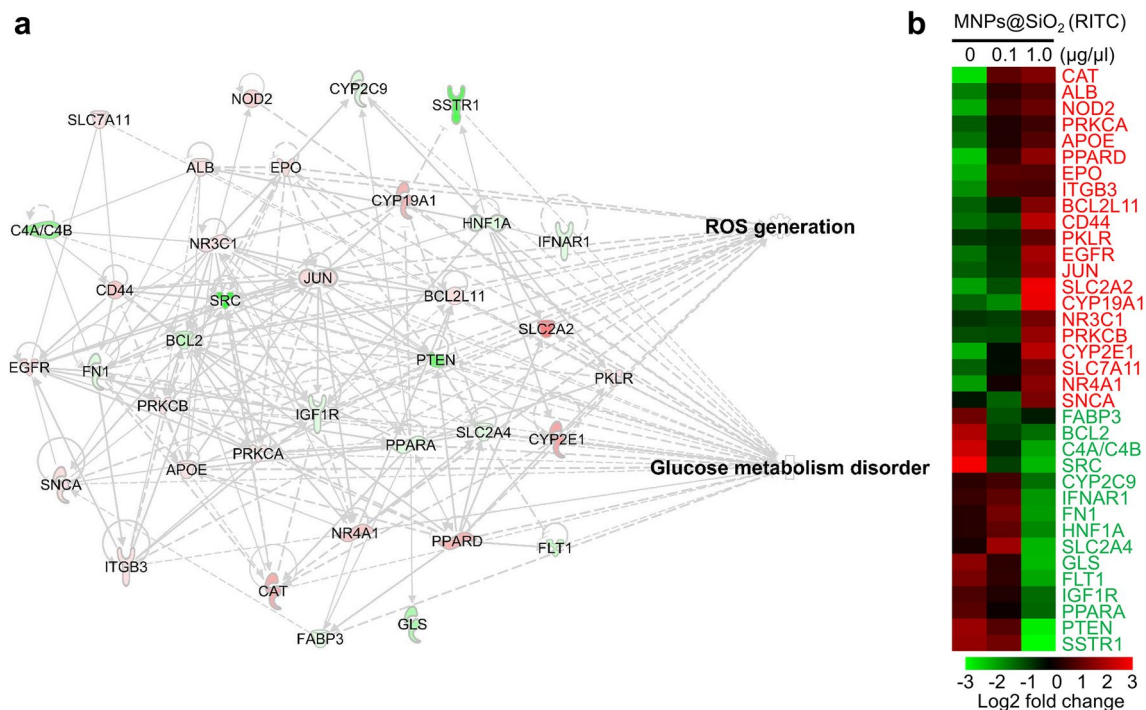


Fig. 4 Transcriptomic disturbance in 1.0 µg/µl MNPs@SiO₂(RITC)-treated HEK293 cells. **a** Functional analysis of the transcriptomic network in 1.0 µg/µl MNPs@SiO₂(RITC)-treated HEK293 cells. The analysis used a fold-change cut-off value of ±3. **b** Heat map of 36 genes related to reactive oxygen species (ROS) generation and glu-

cose metabolic dysfunction with altered expression in a microarray analysis. Red and green areas indicate genes that were upregulated and downregulated compared to the untreated control group, respectively. (Colour figure online)

Supplementary Fig. 4, and Supplementary Table 3). The transcriptomic network predicted increased ROS generation and glucose metabolic dysfunction after treatment with 1.0 µg/µl MNPs@SiO₂(RITC) (Supplementary Fig. 5). In the 1.0 µg/µl MNPs@SiO₂(RITC)-treated group, expression levels of 36 genes were changed compared to control cells; 21 genes were upregulated and 15 genes were downregulated. In the 0.1 µg/µl MNPs@SiO₂(RITC)-treated group, only 14 genes were upregulated and 7 genes were downregulated (Fig. 4b).

Next, we integrated the metabolomic and transcriptomic networks based on biological functions, ROS generation, and glucose metabolic dysfunction. The metabolome and transcriptome were interconnected with strong relationships between biological functions in the 0.1 and 1.0 µg/µl MNPs@SiO₂(RITC)-treated groups (Fig. 5a and Supplementary Fig. 6). The metabotranscriptomic network predicted increased ROS generation and glucose metabolic dysfunction in a manner that was more pronounced than in any single omics network (Supplementary Fig. 7). Thus, we hypothesised that treatment with 1.0 µg/µl MNPs@SiO₂(RITC) would alter glucose metabolism in vitro. In an experimental analysis, treatment with 1.0 µg/µl MNPs@SiO₂(RITC) decreased the efficiency of glucose uptake by 40% compared to treatment with 0.1 µg/µl MNPs@

SiO₂(RITC) or untreated control cells (Fig. 5b). Similarly, intracellular glucose decreased by 30% after treatment with 1.0 µg/µl MNPs@SiO₂(RITC) compared to treatment with 0.1 µg/µl MNPs@SiO₂(RITC) or untreated control cells (Fig. 5c). However, there were no changes in the residual amount of glucose in media (Fig. 5d).

Glucose uptake-related metabolites and genes in the metabotranscriptomic network

Given the observation that reductions in the amount of intracellular glucose were caused by decreased uptake efficiency, we reanalysed the proposed metabotranscriptomic network with the cellular function “glucose uptake”. This query identified 11 directly related factors: 3 AAs and 8 genes (Fig. 6a and Supplementary Fig. 8). The network predicted high suppression of glucose uptake as a result of up- and downregulated metabolites and genes after treatment with 1.0 µg/µl MNPs@SiO₂(RITC) (Supplementary Fig. 9). The metabolites cysteine, lysine, and tyrosine were more closely related to glucose uptake than others.

Based on the prediction results, we quantified changes in the expression of 4 genes using quantitative real-time PCR (Fig. 6b). Gene expression of HNF1 homeobox A (*HNF1A*) was significantly downregulated in 1.0 µg/µl

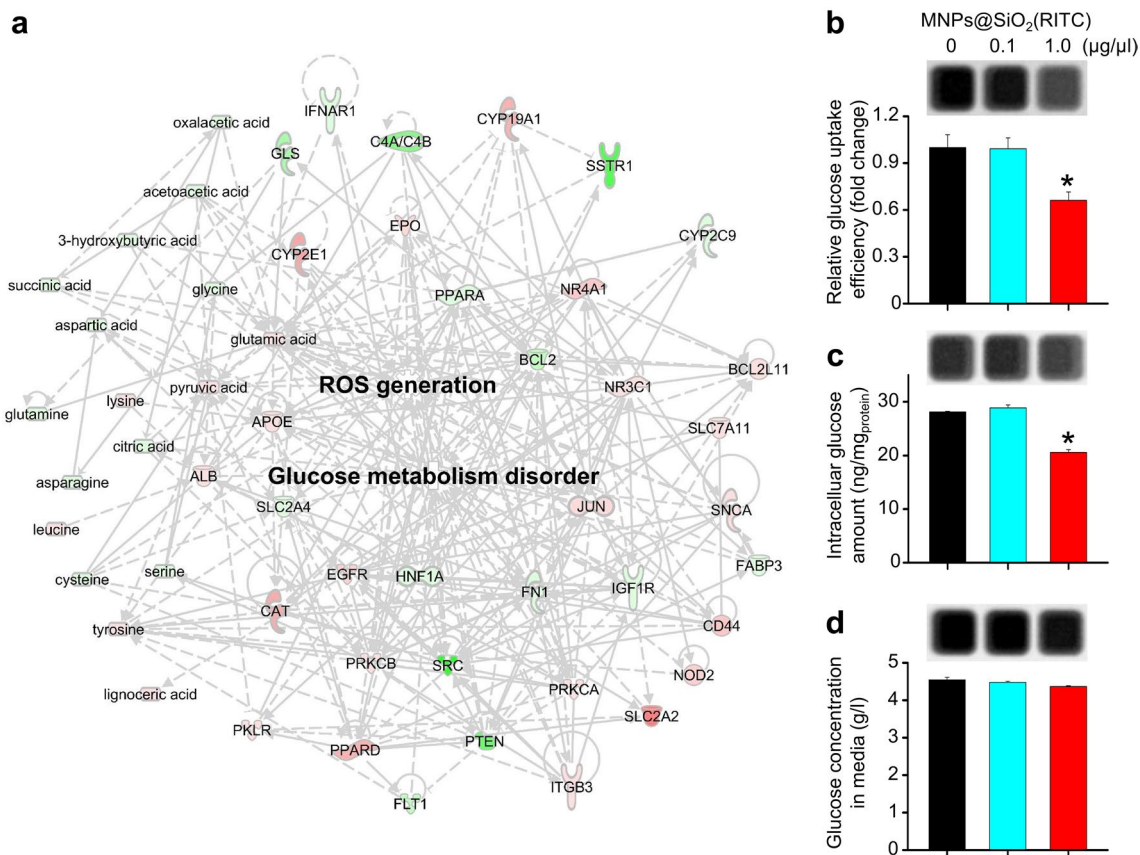


Fig. 5 Metabotranscriptomic network, evaluation of glucose uptake efficiency, and determination of glucose concentration in MNPs@SiO₂(RITC)-treated cells. **a** The analysis used fold-change cut-off values of ± 1.2 for metabolites and ± 3 for genes. Red and green areas indicate upregulated and downregulated factors compared to the

untreated control group, respectively. Glucose uptake efficiency (**b**) and glucose determination in MNPs@SiO₂(RITC)-treated cells (**c**) and media (**d**) were determined on luminescent images. Data represent the mean \pm standard deviation of 3 independent experiments. * $p < 0.05$ vs. untreated control. (Colour figure online)

MNPs@SiO₂(RITC)-treated cells compared to 0.1 µg/µl MNPs@SiO₂(RITC)-treated and untreated control cells. Alternatively, the gene expression levels of nuclear receptor subfamily 4 group A member 1 (*NR4A1*), protein kinase C alpha (*PRKCA*), and solute carrier family 2 member 2 (*SLC2A2*) significantly increased in 1.0 µg/µl MNPs@SiO₂(RITC)-treated cells compared to 0.1 µg/µl MNPs@SiO₂(RITC)-treated and untreated control cells.

To analyse the efficiency of glucose uptake visually, we used fluorescent d-glucose analogue 2-[N-(7-nitrobenz-2-oxa-1,3-diazol-4-yl)amino]-2-deoxy-d-glucose (2-NBDG) as a tracer (Yamada et al. 2000). Since 2-NBDG uptake is mediated through glucose transporter, its uptake has been used for monitoring glucose uptake into cells. We found that glucose uptake efficiency of cells was decreased in 1.0 µg/µl MNPs@SiO₂(RITC)-treated cells compared to 0.1 µg/µl MNPs@SiO₂(RITC)-treated and untreated control cells (Fig. 6c).

Discussion

The present study used an integrated omics-based approach to investigate NP-induced cellular and glucose metabolic dysfunction. Specifically, we investigated the metabolome and transcriptome in NP-treated cells to identify important mechanisms of nanotoxicity and performed a functional metabotranscriptomics analysis to deduce the relationship between ROS generation and glucose metabolic dysfunction after NP exposure. Additionally, we demonstrated that “overdose” (high-concentration) treatment with MNPs@SiO₂(RITC) deregulated glucose metabolism by preventing glucose uptake. Our results indicate that minimizing NP usage or exposure is important for preventing nanotoxicity related to glucose metabolic dysfunction and transport.

In the present study, we simultaneously profiled OAs, AAs, and FAs as EOC/MO/TBDMS derivatives using

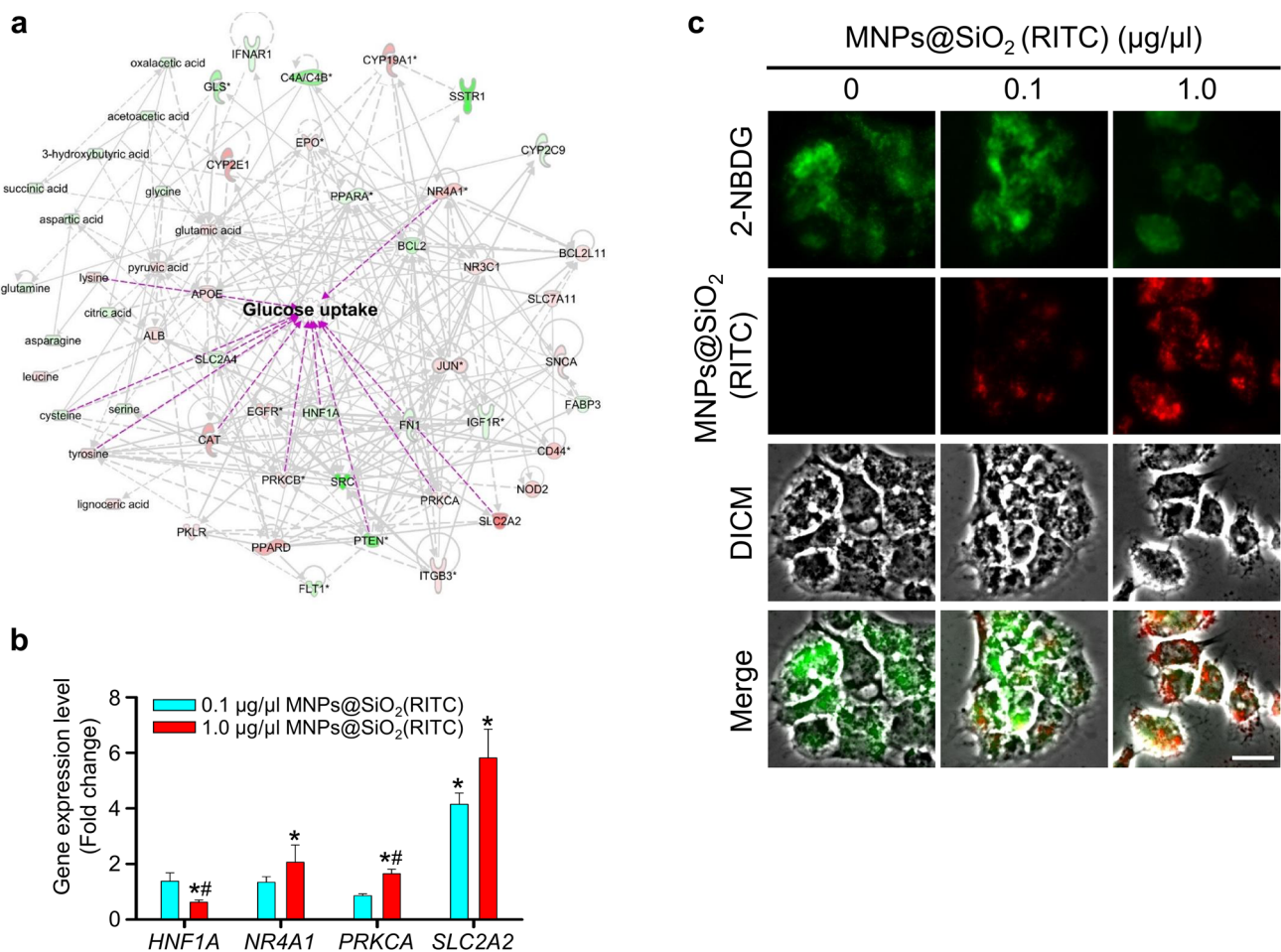


Fig. 6 Functional analysis of the metabolotranscriptomic network for glucose uptake. **a** A second metabolotranscriptomic network analysis was performed for glucose uptake. The analysis used fold-change cut-off values of ± 1.2 for metabolites and ± 3 for genes. Red and green areas indicate upregulated and downregulated factors compared to the untreated control group, respectively. Factors directly related to glucose uptake are highlighted in magenta. **b** A qPCR analysis was

performed to determine glucose uptake-related gene expression in each group using *GAPDH* as an internal control. Data represent the mean \pm standard deviation of 3 independent experiments. * $p < 0.05$ vs. untreated control and # $p < 0.05$ vs. 0.1 $\mu\text{g}/\mu\text{l}$ MNP@SiO₂(RITC). **c** A visual analysis for glucose uptake efficiency of cells was performed using 2-NBDG. Scale bar = 20 μm . (Colour figure online)

GC-MS/MS, which has better sensitivity and accuracy than GC-MS used in previous studies (Phukan et al. 2016; Shim et al. 2012). This allowed shorter analytical times and the simultaneous analysis of 44 metabolites in a single run, which was useful for the rapid and exact monitoring of metabolic alterations after MNP@SiO₂(RITC) treatment.

Changes in cell metabolic profiles can reflect the impairment of redox status, energy metabolism, and biogenesis (Johnson et al. 2016). Previous studies suggest that MNP@SiO₂(RITC) exposure induces ROS generation and mitochondrial damage as well as related metabolic disturbances in OAs, AAs, and polyamine (Phukan et al. 2016; Shim et al. 2012). OA profiles are more vulnerable to ROS and mitochondrial damage than other metabolites because the Krebs cycle occurs in mitochondria and utilises redox reactions for

electron transfer and the generation of adenosine triphosphate (ATP) (Mailloux et al. 2014). We previously reported that the metabolic disturbance of OAs contributed to the accumulation of glutamic acid in MNP@SiO₂(RITC)-treated cells (Shim et al. 2012). In this study, we found that pyruvate showed the largest alterations among all OAs after MNP@SiO₂(RITC) exposure; importantly, pyruvate is the final product of glycolysis in the cytosol. In subsequent steps of energy metabolism, pyruvate is transported into mitochondria via pyruvate translocase to interact with pyruvate dehydrogenase, which converts pyruvate into acetyl-CoA on the inner membrane of the mitochondrial matrix (Stacpoole et al. 2003; Sutendra et al. 2014). We previously demonstrated structural disintegration and depolarization in mitochondria following MNP@SiO₂(RITC) treatment (Shim et al. 2012). These mitochondrial effects may contribute to

the accumulation of pyruvate and thus glucose metabolic dysfunction in MNPs@SiO₂(RITC)-treated cells.

Changes in AA profiles can signal homeostatic deregulation (Chaveroux et al. 2009). We previously demonstrated that increases in glutamic acid after MNPs@SiO₂(RITC) treatment were caused by changes in metabolic pathway-related genes and associated OA profiles. Additionally, free AAs such as tryptophan, tyrosine, histidine, and cysteine are directly oxidized by ROS (Droge 2002). Glycine attenuates superoxide anion radical release in the presence of nicotinamide adenine dinucleotide phosphate and decreases protein carbonyl and lipid peroxidation by promoting levels of glutathione synthetase and, consequently, glutathione (Ruiz-Ramirez et al. 2014). ROS generation is increased by the accumulation of basic AAs such as arginine, ornithine, and lysine in the mitochondrial membrane and induces mitochondria-dependent cell death via aberrant ubiquitination (Braun et al. 2015). In this study, we found that 1.0 µg/µl MNPs@SiO₂(RITC) significantly increased levels of leucine, glutamic acid, lysine, and tyrosine and decreased those of glycine, serine, cysteine, and glutamine in HEK293 cells. These changes may be closely related to MNPs@SiO₂(RITC)-induced ROS generation.

Our study had a limited ability to assess changes in FAs, although some MNPs@SiO₂(RITC)-associated changes were detected compared to the control group. FA levels are highly related to ROS generation and have important roles in cellular function. ROS can oxidize polyunsaturated phospholipids, glycolipids, and cholesterol membrane components to impair plasma membrane function (Girotti 1998). Malondialdehyde, acrolein, and 4-hydroxynonenal are generated from the oxidative cleavage of polyunsaturated phospholipids (Negre-Salvayre et al. 2008) and deplete unsaturated phospholipids and cholesterol. In this study, we were unable to identify consistent changes in gene patterns due to the limitations of our bioinformatics database.

In the present study, we made deductions and connections based on the datasets of differentially expressed genes and metabolites to generate a metabotranscriptomic network. Cysteine and lysine have been associated with glucose transporter protein expression (Gazit et al. 2003; Katsumata 2011), and tyrosine reversibly inhibits glucose transporter function (Widmer et al. 1990). Moreover, ROS directly oxidize cysteine to generate cystine, a dimer form of cysteine (Droge 2002). In our study, the contribution of decreased cysteine availability to the metabotranscriptomic network predictions in the 1.0 µg/µl MNPs@SiO₂(RITC) treatment condition was potentially related to its involvement in glucose uptake and the sensitivity of cysteine to ROS generation. In the gene expression analysis, *HNF1A*, a transcriptional regulator of *SLC2A2* (Bae et al. 2010), was significantly downregulated after treatment with 1.0 µg/µl MNPs@SiO₂(RITC). Additionally, there were significant

increases in the expression of *NR4A1*, which controls the expression of key metabolic genes for glucose transportation, insulin signalling, glycolysis, and glycogenolysis (Corrocher et al. 2017). *PRKCA* is a kinase involved in glucose transporter activation (Lee et al. 2015) and *SLC2A2*, also known as glucose transporter 2 (*GLUT2*), is a bidirectional glucose transporter that is responsible for the bulk of glucose transportation in the cell (Mueckler and Thorens 2013). *SLC2A2* and its regulator gene, *NR4A1*, are transcriptionally and translationally sensitive to oxidative stress (Lee et al. 2014; Shimizu et al. 2015; Shirakawa and Terauchi 2014). We presume that these disturbances in metabolic profiles and the transcriptome converge to explain increased ROS generation and glucose metabolic dysfunction after MNPs@SiO₂(RITC) exposure in vitro.

Even though kidneys are known to particularly susceptible to nanotoxicity due to nanoparticles accumulation and these are one of the main elimination routes of nanoparticles in vivo (Iavicoli et al. 2016), our investigation is limited in kidney-derived cell lines treated with nanoparticle. Therefore, further studies are needed concerning the effect of nanoparticles on primary kidney cells and in vivo before biomedical applications.

In conclusion, our findings indicate that exposure to high concentrations of NPs can be deleterious to glucose metabolism and cellular glucose uptake. These results highlight important safety considerations for nanotoxicity when using NPs for therapeutic or diagnostic purposes.

Acknowledgements This work was supported by the Brain Research Program through the National Research Foundation of Korea (NRF) funded by the Ministry of Science, ICT & Future Planning (2016M3C7A1904392, 2015R1A4A1041219), the Intelligent Synthetic Biology Center of Global Frontier Project funded by the Ministry of Science, ICT & Future Planning (2014M3A6A8066439), and Ministry of Food and Drug Safety (14182MFD5978).

Compliance with ethical standards

Conflict of interest The authors declare that they have no conflict of interest.

Open Access This article is distributed under the terms of the Creative Commons Attribution 4.0 International License (<http://creativecommons.org/licenses/by/4.0/>), which permits unrestricted use, distribution, and reproduction in any medium, provided you give appropriate credit to the original author(s) and the source, provide a link to the Creative Commons license, and indicate if changes were made.

References

- Bae JS, Kim TH, Kim MY, Park JM, Ahn YH (2010) Transcriptional regulation of glucose sensors in pancreatic beta-cells and liver: an update. *Sensors* (Basel) 10(5):5031–5053. <https://doi.org/10.3390/s100505031>

- Bahillo-Curienes MP, Garrote-Molpeceres R, Minambres-Rodriguez M, Del Real-Llorente MR, Tobar-Mideros C, Rellán-Rodriguez S (2017) Glycosuria and hyperglycemia in the neonatal period as the first clinical sign of Fanconi-Bickel syndrome. *Pediatr Diabetes*. <https://doi.org/10.1111/pedi.12531>
- Beck GR, Ha SW, Camalier CE et al (2012) Bioactive silica-based nanoparticles stimulate bone-forming osteoblasts, suppress bone-resorbing osteoclasts, and enhance bone mineral density in vivo. *Nanomedicine* 8(6):793–803. <https://doi.org/10.1016/j.nano.2011.11.003>
- Braun RJ, Sommer C, Leibiger C et al (2015) Accumulation of basic amino acids at mitochondria dictates the cytotoxicity of aberrant ubiquitin. *Cell Rep*. <https://doi.org/10.1016/j.celrep.2015.02.009>
- Cersosimo E, Solis-Herrera C, Triplitt C (2014) Inhibition of renal glucose reabsorption as a novel treatment for diabetes patients. *J Bras Nefrol* 36(1):80–92
- Chaveroux C, Jousse C, Cherasse Y et al (2009) Identification of a novel amino acid response pathway triggering ATF2 phosphorylation in mammals. *Mol Cell Biol* 29(24):6515–6526. <https://doi.org/10.1128/MCB.00489-09>
- Corrocher FA, Bueno de Paiva L, Duarte ASS et al (2017) Reduced expression of NR4A1 activates glycolytic pathway in acute promyelocytic leukemia cells. *Leuk Lymphoma*:1–4 <https://doi.org/10.1080/10428194.2017.1387900>
- DeFronzo RA, Davidson JA, Del Prato S (2012) The role of the kidneys in glucose homeostasis: a new path towards normalizing glycaemia. *Diabetes Obes Metab* 14(1):5–14. <https://doi.org/10.1111/j.1463-1326.2011.01511.x>
- Delyagina E, Schade A, Scharfenberg D et al (2014) Improved transfection in human mesenchymal stem cells: effective intracellular release of pDNA by magnetic polyplexes. *Nanomedicine (Lond)* 9(7):999–1017. <https://doi.org/10.2217/nmm.13.71>
- Ding YF, Li S, Liang L et al (2018) Highly biocompatible chlorin e6-loaded chitosan nanoparticles for improved photodynamic cancer therapy. *ACS Appl Mater Interfaces* 10(12):9980–9987. <https://doi.org/10.1021/acsami.8b01522>
- Droge W (2002) Free radicals in the physiological control of cell function. *Physiol Rev* 82(1):47–95. <https://doi.org/10.1152/physrev.00018.2001>
- Evans TG (2015) Considerations for the use of transcriptomics in identifying the ‘genes that matter’ for environmental adaptation. *J Exp Biol* 218(Pt 12):1925–1935. <https://doi.org/10.1242/jeb.114306>
- Gazit V, Ben-Abraham R, Vofsi O, Katz Y (2003) L-cysteine increases glucose uptake in mouse soleus muscle and SH-SY5Y cells. *Metab Brain Dis* 18(3):221–231
- Gibney MJ, Walsh M, Brennan L, Roche HM, German B, van Ommen B (2005) Metabolomics in human nutrition: opportunities and challenges. *Am J Clin Nutr* 82(3):497–503
- Girotti AW (1998) Lipid hydroperoxide generation, turnover, and effector action in biological systems. *J Lipid Res* 39(8):1529–1542
- Iavicoli I, Fontana L, Nordberg G (2016) The effects of nanoparticles on the renal system. *Crit Rev Toxicol* 46(6):490–560. <https://doi.org/10.1080/10408444.2016.1181047>
- Ito A, Honda H, Kobayashi T (2006) Cancer immunotherapy based on intracellular hyperthermia using magnetite nanoparticles: a novel concept of “heat-controlled necrosis” with heat shock protein expression. *Cancer Immunol Immunother* 55(3):320–328. <https://doi.org/10.1007/s00262-005-0049-y>
- Jain RK, Stylianopoulos T (2010) Delivering nanomedicine to solid tumors. *Nat Rev Clin Oncol* 7(11):653–664. <https://doi.org/10.1038/nrclinonc.2010.139>
- Johnson CH, Ivanisevic J, Siuzdak G (2016) Metabolomics: beyond biomarkers and towards mechanisms. *Nat Rev Mol Cell Biol* 17(7):451–459. <https://doi.org/10.1038/nrm.2016.25>
- Katsumata M (2011) Promotion of intramuscular fat accumulation in porcine muscle by nutritional regulation. *Anim Sci J* 82(1):17–25. <https://doi.org/10.1111/j.1740-0929.2010.00844.x>
- Krug HF, Wick P (2011) Nanotoxicology: an interdisciplinary challenge. *Angew Chem Int Ed Engl* 50(6):1260–1278. <https://doi.org/10.1002/anie.201001037>
- Lai X, Wei Y, Zhao H et al (2015) The effect of Fe₂O₃ and ZnO nanoparticles on cytotoxicity and glucose metabolism in lung epithelial cells. *J Appl Toxicol* 35(6):651–664. <https://doi.org/10.1002/jat.3128>
- Lee SO, Jin UH, Kang JH et al (2014) The orphan nuclear receptor NR4A1 (Nur77) regulates oxidative and endoplasmic reticulum stress in pancreatic cancer cells. *Mol Cancer Res* 12(4):527–538. <https://doi.org/10.1158/1541-7786.MCR-13-0567>
- Lee EE, Ma J, Sacharidou A et al (2015) A protein kinase C phosphorylation motif in GLUT1 affects glucose transport and is mutated in GLUT1 deficiency syndrome. *Mol Cell* 58(5):845–853. <https://doi.org/10.1016/j.molcel.2015.04.015>
- Mailloux RJ, Jin X, Willmore WG (2014) Redox regulation of mitochondrial function with emphasis on cysteine oxidation reactions. *Redox Biol* 2:123–139. <https://doi.org/10.1016/j.redox.2013.12.011>
- Meng H, Xia T, George S, Nel AE (2009) A predictive toxicological paradigm for the safety assessment of nanomaterials. *ACS Nano* 3(7):1620–1627. <https://doi.org/10.1021/nn9005973>
- Mueckler M, Thorens B (2013) The SLC2 (GLUT) family of membrane transporters. *Mol Aspects Med* 34(2–3):121–138. <https://doi.org/10.1016/j.mam.2012.07.001>
- Negre-Salvayre A, Coatrieux C, Ingueneau C, Salvayre R (2008) Advanced lipid peroxidation end products in oxidative damage to proteins. Potential role in diseases and therapeutic prospects for the inhibitors. *Br J Pharmacol* 153(1):6–20. <https://doi.org/10.1038/sj.bjp.0707395>
- Paik MJ, Kim KR (2004) Sequential ethoxycarbonylation, methoximation and tert-butyltrimethylsilylation for simultaneous determination of amino acids and carboxylic acids by dual-column gas chromatography. *J Chromatogr A* 1034(1–2):13–23
- Paik MJ, Lee HJ, Kim KR (2005) Simultaneous retention index analysis of urinary amino acids and carboxylic acids for graphic recognition of abnormal state. *J Chromatogr B Analyt Technol Biomed Life Sci* 821(1):94–104. <https://doi.org/10.1016/j.jchromb.2005.04.011>
- Park KS, Tae J, Choi B et al (2010) Characterization, in vitro cytotoxicity assessment, and in vivo visualization of multimodal, RITC-labeled, silica-coated magnetic nanoparticles for labeling human cord blood-derived mesenchymal stem cells. *Nanomed Nanotechnol Biol Med* 6(2):263–276
- Phukan G, Shin TH, Shim JS et al (2016) Silica-coated magnetic nanoparticles impair proteasome activity and increase the formation of cytoplasmic inclusion bodies in vitro. *Sci Rep* 6:29095. <https://doi.org/10.1038/srep29095>
- Qi R, Wang Y, Bruno PM et al (2017) Nanoparticle conjugates of a highly potent toxin enhance safety and circumvent platinum resistance in ovarian cancer. *Nat Commun* 8(1):2166. <https://doi.org/10.1038/s41467-017-02390-7>
- Rehrauer H, Opitz L, Tan G, Sieverling L, Schlapbach R (2013) Blind spots of quantitative RNA-seq: the limits for assessing abundance, differential expression, and isoform switching. *BMC Bioinformatics* 14:370. <https://doi.org/10.1186/1471-2105-14-370>
- Ruiz-Ramirez A, Ortiz-Balderas E, Cardozo-Saldana G, Diaz-Diaz E, El-Hafidi M (2014) Glycine restores glutathione and protects against oxidative stress in vascular tissue from sucrose-fed rats. *Clin Sci (Lond)* 126(1):19–29. <https://doi.org/10.1042/CS20130164>
- Shim W, Paik MJ, Nguyen DT et al (2012) Analysis of changes in gene expression and metabolic profiles induced by silica-coated

- magnetic nanoparticles. *ACS Nano* 6(9):7665–7680. <https://doi.org/10.1021/nn301113f>
- Shimizu Y, Miyakura R, Otsuka Y (2015) Nuclear receptor subfamily 4, group A, member 1 inhibits extrinsic apoptosis and reduces caspase-8 activity in H₂O₂-induced human HUC-F2 fibroblasts. *Redox Rep* 20(2):81–88. <https://doi.org/10.1179/1351000214Y.0000000109>
- Shin TH, Lee DY, Lee HS et al (2018) Integration of metabolomics and transcriptomics in nanotoxicity studies. *BMB Rep* 51:14
- Shirakawa J, Terauchi Y (2014) Selective and sequential loss of transcriptional factors: a hallmark of beta-cell failure in type 2 diabetes? *J Diabetes Investig* 5(4):359–361. <https://doi.org/10.1111/jdi.12212>
- Silva MM, Calado R, Marto J, Bettencourt A, Almeida AJ, Goncalves LMD (2017) Chitosan nanoparticles as a mucoadhesive drug delivery system for ocular administration. *Mar Drugs* 15(12) <https://doi.org/10.3390/md15120370>
- Stacpoole PW, Owen R, Flotte TR (2003) The pyruvate dehydrogenase complex as a target for gene therapy. *Curr Gene Ther* 3(3):239–245
- Stark WJ (2011) Nanoparticles in biological systems. *Angew Chem Int Ed Engl* 50(6):1242–1258. <https://doi.org/10.1002/anie.200906684>
- Sutendra G, Kinnaird A, Dromparis P et al (2014) A nuclear pyruvate dehydrogenase complex is important for the generation of acetyl-CoA and histone acetylation. *Cell* 158(1):84–97. <https://doi.org/10.1016/j.cell.2014.04.046>
- Van Assche R, Broeckx V, Boonen K et al (2015) Integrating-Omics: systems biology as explored through *C. elegans* research. *J Mol Biol* 427(21):3441–3451. <https://doi.org/10.1016/j.jmb.2015.03.015>
- Wang F, Gao F, Lan M, Yuan H, Huang Y, Liu J (2009) Oxidative stress contributes to silica nanoparticle-induced cytotoxicity in human embryonic kidney cells. *Toxicol In Vitro* 23(5):808–815. <https://doi.org/10.1016/j.tiv.2009.04.009>
- Widmer J, Raffin Y, Gaillard JM, Bovier P, Tissot R (1990) Reversible in vitro decrease of L-tyrosine and L-tryptophan influx across the human erythrocyte membrane induced by cytochalasin B, the specific inhibitor of D-glucose transport. *Neuropsychobiology* 24(2):67–73
- Yamada K, Nakata M, Horimoto N, Saito M, Matsuoka H, Inagaki N (2000) Measurement of glucose uptake and intracellular calcium concentration in single, living pancreatic beta-cells. *J Biol Chem* 275(29):22278–22283. <https://doi.org/10.1074/jbc.M908048199>
- Yoon TJ, Kim JS, Kim BG, Yu KN, Cho MH, Lee JK (2005) Multifunctional nanoparticles possessing a “magnetic motor effect” for drug or gene delivery. *Angew Chem Int Ed Engl* 44(7):1068–1071. <https://doi.org/10.1002/anie.200461910>
- Zhang Q, Xu H, Zheng S, Su M, Wang J (2015) Genotoxicity of mesoporous silica nanoparticles in human embryonic kidney 293 cells. *Drug Test Anal* 7(9):787–796. <https://doi.org/10.1002/dta.1773>

Publisher's Note Springer Nature remains neutral with regard to jurisdictional claims in published maps and institutional affiliations.